
Learning Solution-Aware Transformers for Efficiently Solving Quadratic Assignment Problem

Zhentao Tan^{1,2} Yadong Mu²

Abstract

Recently various optimization problems, such as Mixed Integer Linear Programming Problems (MILPs), have undergone comprehensive investigation, leveraging the capabilities of machine learning. This work focuses on learning-based solutions for efficiently solving the Quadratic Assignment Problem (QAPs), which stands as a formidable challenge in combinatorial optimization. While many instances of simpler problems admit fully polynomial-time approximate solution (FPTAS), QAP is shown to be strongly NP-hard. Even finding a FPTAS for QAP is difficult, in the sense that the existence of a FPTAS implies $P = NP$. Current research on QAPs suffer from limited scale and computational inefficiency. To attack the aforementioned issues, we here propose the first solution of its kind for QAP in the learn-to-improve category. This work encodes facility and location nodes separately, instead of forming computationally intensive association graphs prevalent in current approaches. This design choice enables scalability to larger problem sizes. Furthermore, a Solution AWAre Transformer (SAWT) architecture integrates the incumbent solution matrix with the attention score to effectively capture higher-order information of the QAPs. Our model’s effectiveness is validated through extensive experiments on self-generated QAP instances of varying sizes and the QAPLIB benchmark.

in diverse real-world applications. This includes in-depth studies related to vehicle routing problems (VRPs) (Veres & Moussa, 2020), chip placement and routing problems (Mirhoseini et al., 2021; Lai et al., 2022; Tan & Mu, 2024), and molecule learning (Ahn et al., 2020; Yang et al., 2023). Given the NP-hard nature of COPs, conventional solvers and manually crafted heuristics face challenges in finding optimal solutions. Consequently, there has been a recent emergence of machine learning based methods aimed at swiftly identifying sub-optimal solutions, proving notably successful in this pursuit.

Given the discrete nature of COPs, reinforcement learning (RL) proves instrumental in their resolution, either by constructing solutions in learn-to-construct (L2C) methods (Vinyals et al., 2015; Kwon et al., 2020) or improving initial solutions iteratively in learn-to-improve (L2I) solvers (Ma et al., 2021; 2023). Despite the prevalent focus on mixed integer linear programming problems (MILPs), particularly in solving VRPs (Zhang et al., 2023), machine learning applications to QAPs remain relatively sparse in current literature.

For QAPs, prevalent machine learning approaches focus on graph matching (Nowak et al., 2018; Wang et al., 2021; Liu et al., 2022). Specifically, (Wang et al., 2021) utilizes an association graph to address QAPs with a complexity of $O(n^4)$ for instances of size n , limiting its applicability to only small problem size (*e.g.*, below 30). Moreover, it requires labeled data for training, impractical for larger QAP sizes. Following (Wang et al., 2021), the work in (Liu et al., 2022) employs L2C reinforcement learning methods for QAPs without requiring ground truth, yet scalability challenges persist. In contrast, traditional Operations Research (OR) approaches (Zhang et al., 2020; Mihalčić et al., 2018) rely on meta-heuristic search strategies. For instance, (Zhang et al., 2020) combines genetic heuristics with tabu-search, and (Mihalčić et al., 2018) adopts an adaptive large neighbor search strategy. However, these methods often demand hours to find the optimal solution for a single instance, rendering them inefficient.

To address the outlined challenges, we propose a novel L2I approach that integrates reinforcement learning with a Solution Aware Transformer (SAWT) model to tackle

1. Introduction

Combinatorial Optimization Problems (COPs) involving discrete variables as input have garnered substantial attention

¹Center for Data Science, Peking University, China.

²Wangxuan Institute of Computer Technology, Peking University, China. Correspondence to: Yadong Mu <myd@pku.edu.cn>.

Koopmans-Beckmann’s Quadratic Assignment Problem. This method adeptly handles QAP instances of various sizes. To eliminate the need for an association graph, we employ a mixed-score Transformer and a Graph Convolution Network (GCN) to independently encode facility and location nodes, enabling scalability to larger problem sizes. Our SAWT encoder dynamically captures graph structure patterns in the QAP, adapting to different assignment solutions. The decoder facilitates refinement by executing swap operations between two positions within the assignment solution, enhancing overall quality. Extensive experiments on self-generated QAP instances and QAPLIB (Burkard et al., 1997) benchmarks showcase the model’s effectiveness and robust generalization to instances of varying sizes. Most importantly, to our best knowledge, the proposed method is the first L2I method of its kind to solve the QAP.

The paper makes the following key contributions: (1) Introducing the first learn-to-improve reinforcement learning method for the Quadratic Assignment Problem, exhibiting proficiency in solving instances up to a size of 100. (2) Proposing a novel Solution Aware Transformer (SAWT) model adept at effectively capturing QAP patterns through the dynamic integration of solution-aware information into the attention model. (3) Through extensive experiments on self-generated Koopmans-Beckmann’s QAP instances and QAPLIB benchmarks, showing the SAWT model’s efficient QAP-solving capabilities and robust generalization across various instances.

2. Quadratic Assignment Problem

As per the definition in (Koopmans & Beckmann, 1957), a QAP involves the optimal assignment of n facilities to n locations. Represented with a facility set \mathbf{Fac} and a location set \mathbf{Loc} , the Koopmans-Beckmann’s QAP is defined as below:

$$\begin{aligned} \min_x \quad & \sum_{i,j=1}^n \sum_{k,p=1}^n f_{ij} d_{kp} x_{ik} x_{jp}, \\ \text{s.t.} \quad & \sum_{i=1}^n x_{ij} = 1, \quad 1 \leq j \leq n, \\ & \sum_{j=1}^n x_{ij} = 1, \quad 1 \leq i \leq n, \\ & x_{ij} \in \{0, 1\}, \quad 1 \leq i, j \leq n, \end{aligned} \quad (1)$$

where f_{ij} is the flow from facility fac_i to facility fac_j , and d_{kp} is the distance between locations loc_k and location loc_p . x_{ik} is a binary variable indicating whether to place facility fac_i to location loc_k or not. The constraints in Definition 1 stipulate the exclusive assignment of one facility to a single location. Another prevalent QAP formulation is presented

in trace format (Edwards, 1980):

$$\begin{aligned} \min_{\mathbf{X}} \quad & \text{trace}(\mathbf{F} \cdot \mathbf{X} \cdot \mathbf{D} \cdot \mathbf{X}^T), \\ \text{s.t.} \quad & \mathbf{X} \cdot \mathbf{1} = \mathbf{1}, \mathbf{X}^T \cdot \mathbf{1} = \mathbf{1}, \\ & \mathbf{X} \in \{0, 1\}^{n \times n}, \end{aligned} \quad (2)$$

where \mathbf{F} and \mathbf{D} are flow or distance matrix, respectively. \mathbf{X} is a permutation matrix and $\mathbf{1}$ is an all-one vector. For clarity, we set the objective function for the QAP as $L(\mathbf{X}) = \text{trace}(\mathbf{F} \cdot \mathbf{X} \cdot \mathbf{D} \cdot \mathbf{X}^T)$.

The QAP finds relevance in diverse real-world applications. For instance, it has applications in electronic module placement (Steinberg, 1961), where f_{ij} denotes connections between modules i and j , and d_{kp} signifies distances between locations k and p , allowing for the minimization of total electrical connection length. Additionally, QAP was also utilized in hospital room assignment scenarios (Elshafei, 1977), where f_{ij} represents patient transfers between rooms, and d_{ij} indicates travel time from room i to room j . Other applications include imagery (Taillard, 1991) and turbine runner balancing (Laporte & Mercure, 1988). For further details, interested readers can refer to the provided references.

Critically, solving the QAP is challenging, as evidenced by (Sahni & Gonzalez, 1976), which establishes the absence of a polynomial algorithm with ϵ -approximation unless $P = NP$. Notably, QAP, encompassing the well-studied Traveling Salesman Problem (TSP) as a special case, emerges as a more intricate problem. Despite its widespread application, the current deep learning landscape has shown limited attention to QAP. Considering the real-world significance and inherent complexities, we posit that deep learning methods can play a substantial role in addressing and influencing solutions for QAPs.

3. Related Work

Traditional methods for QAP: Koopmans-Beckmann’s QAP has received significant attention in the Operations Research (OR) community. Genetic algorithms (Hanh et al., 2019; Ahmed, 2015) were probability search methods based on biological principles of natural selection, recombination, mutation, and survival of the fittest. Tabu-search algorithms (Zhang et al., 2020; Shylo, 2017; James et al., 2009) were local search methods that utilize a tabu list to prevent duplicate solutions. Other meta-heuristics like large neighborhood search (Mihic et al., 2018; Wang & Alidaee, 2023) and swarm algorithms (Cui et al., 2023) show competitive performance on QAPs. However, these methods, tailored to specific problems, often require hours for solving a single instance, posing challenges for real-world deployment.

Learning-based methods for QAP: Learning-based meth-

ods for QAPs remain limited in the literature. The majority of existing works focus on graph matching (Zanfir & Sminchisescu, 2018; Yu et al., 2021; Lin et al., 2023). The work in (Wang et al., 2021) pioneered supervised learning for QAPs, transforming them into node classification tasks on association graphs, where each node represents a matching pair. Classification of a node as one indicates the selection of that pair for matching. The state-of-the-art work in (Liu et al., 2022) introduced the first learn-to-construct (L2C) reinforcement learning method for QAPs without ground truth, utilizing struct2vec (Dai et al., 2016) for node encoding. However, scalability issues arise due to the $O(n^4)$ complexity of association graphs.

RL for combinatorial optimization: Reinforcement learning for COPs has witnessed extensive recent research. Learn-to-construct (L2C) methods began with (Bello et al., 2017), utilizing PtrNet (Vinyals et al., 2015) for solving Traveling Salesman Problems. Subsequent advancements involved Graph Neural Networks (GNNs) (Khalil et al., 2017), attention models (Kwon et al., 2020) for high-quality solutions in vehicle routing problems, Minimum Vertex Cover, and other COPs. MatNet (Kwon et al., 2021) is the first to take matrix inputs for COP resolution. In learn-to-improve (L2I) methods, (Chen & Tian, 2019) relied on local search, improved by NLNS solver (Wu et al., 2021) with handcrafted operators. Recent approaches focus on controlling k-opt and swap heuristics for VRPs, with (Costa et al., 2020) on 2-opt, (Sui et al., 2021) on 3-opt, and (Ma et al., 2021; 2023) achieving state-of-the-art performance using Transformer and special positional embeddings to capture the linear structure of VRPs. However, these methods lack the capability to address QAPs due to their inability to capture the graph structure within QAPs.

4. Problem Formulation

As explained in Section 2, the solution to a QAP involves creating a one-to-one assignment between facilities and locations that minimizes the total cost. An assignment: $\sigma = (\sigma(1), \dots, \sigma(n))$ is a map where $\sigma : i \rightarrow \sigma(i)$ means mapping facility f_{ac_i} to location $loc_{\sigma(i)}$.

Starting with an initial feasible solution, our deep reinforcement learning model iteratively enhances the solution. The policy initiates by selecting a facility pair $(i, j; i < j)$, and subsequently, a swap operation is applied to the current solution σ , resulting in the next solution $\sigma' = (\sigma(1), \dots, \sigma(j), \dots, \sigma(i), \dots, \sigma(n))$. This swap operation iterates until reaching the step limit T_{limit} , encapsulating the process as a Markov Decision Process (MDP), as depicted below.

States. Following (Costa et al., 2020), we define a state $\bar{\sigma} = (\sigma, \sigma^*)$ where σ and σ^* are the current solution and

current lowest-cost solution respectively. For example, at step t , $\sigma_t^* = \arg \min_{\sigma_{\bar{t}} \in \{\sigma_1, \dots, \sigma_t\}} L(\sigma_{\bar{t}})$.

Actions. The actions in our model are pairs of facilities' indices: $A = (i, j; i < j)$ for the swap operations.

Rewards. The reward function is defined as: $r_t = L(\sigma_t^*) - \min(L(\sigma_t^*), L(\sigma_{t+1}))$. This formulation ensures that the sum of intermediate rewards at each step corresponds to the total decrease in cost relative to the initial solution.

Transitions. Given the action: (i, j) and current solution σ_t , the next solution is generated through swap operation: $\sigma_{t+1} = (\sigma_t(1), \dots, \sigma_t(j), \dots, \sigma_t(i), \dots, \sigma_t(n))$. Note that even if the transition does not improve the objective function, the RL agent will still accept the next solution. By doing this, we can expect the agent to punish non-improving actions by assigning 0 rewards.

Policy. The policy π_θ is parameterized by our SAWT model with the parameter θ . At step t , given the current state σ_t , an action pair $a_t = (i_t, j_t)$ is sampled through $\pi_\theta(a_t | \sigma_t)$. For an episode with a length of T_{limit} starting from the initial solution σ_0 , the process can be expressed as the probability based on the chain rule:

$$P(\sigma_{T_{limit}} | \sigma_0) = \prod_{t=1}^{T_{limit}} \pi_\theta(a_t | \sigma_{t-1}). \quad (3)$$

5. Solution-Aware Transformers

Here we introduce our policy network: Solution Aware Transformer (SAWT). The entire model pipeline is depicted in Figure 1, illustrating the process using a QAP example with 5 facilities and locations. In the SAWT *encoder* module, the SAWT processes the concatenation of embeddings for 5 facilities and locations, incorporating the solution-aware matrix M into the attention module. This design enables our model to dynamically capture information from the incumbent solution. The SAWT *decoder* then utilizes the output from the *encoder* to generate action pairs and critic values.

5.1. Embeddings

To circumvent the need for an association graph, we independently encode facility and location nodes, improving scalability to larger problem sizes.

Location embedding. The initial representation of a location, $loc_i = (x_i, y_i)$, is a 2-dimensional coordinate. We employ a linear projection function on loc_i to obtain a latent representation $loc_i \in \mathbb{R}^d$. Locations form a distance graph so that it is natural to encode them using Graph Convolutional Network (GCN). loc_i is then fed into three layers of a GCN, as defined in Equation 4, using the distance matrix

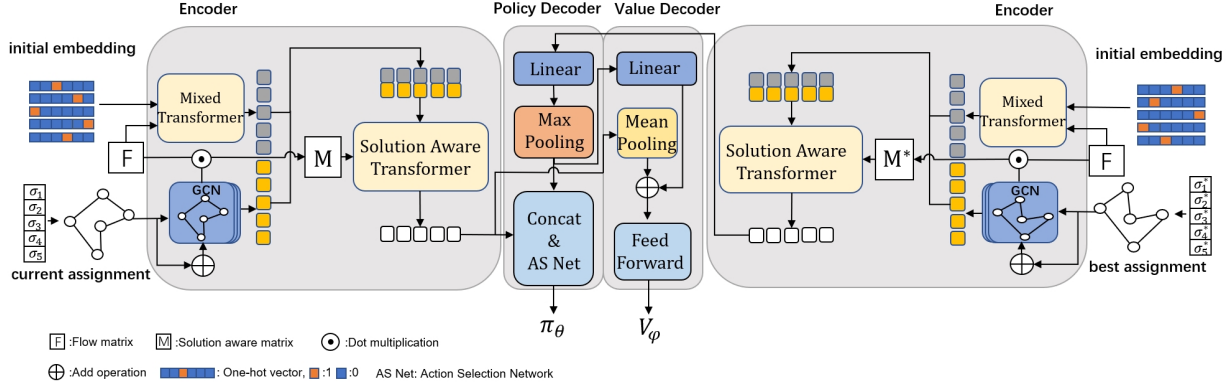


Figure 1. Architecture of our policy network, namely Solution Aware Transformer (SAWT). See main text for more details.

as the affinity matrix, resulting in the final embedding of locations $loc_i \in \mathbb{R}^d$.

$$\mathbf{Loc}^{(l+1)} = \mathbf{Loc}^{(l)} + \text{ReLU}(\mathbf{D} \mathbf{Loc}^{(l)} \mathbf{W}^{(l)}), \quad (4)$$

where $\mathbf{W}^{(l)} \in \mathbb{R}^{d \times d}$ are the trainable parameters and ReLU refers to the Rectified Linear Unit.

Facility embedding. Encoding facility nodes into a higher-dimensional space poses a challenge due to the matrix-type input (flow matrix), which neural networks find difficult to encode. Drawing inspiration from (Kwon et al., 2021), we address this by mixing the flow matrix into the attention score within a Transformer. Initialization of facility nodes’ embeddings fac_i begins with a random one-hot vector of a predefined high dimension $N_{init} \gg n$. The encoding process for facility nodes then follows the equation as shown below:

$$\mathbf{Fac}^{(l+1)} = \text{softmax}(g(\mathbf{Att}(\mathbf{Fac}^{(l)}, \mathbf{Fac}^{(l)}), \mathbf{F}))(\mathbf{Fac}^{(l)} \mathbf{W}^v),$$

$$\mathbf{Att}(\mathbf{Fac}^{(l)}, \mathbf{Fac}^{(l)}) = \frac{(\mathbf{Fac}^{(l)} \mathbf{W}^q)(\mathbf{Fac}^{(l)} \mathbf{W}^k)}{\sqrt{N_{init}}}, \quad (5)$$

where $\mathbf{W}^q \in \mathbb{R}^{N_{init} \times d_q}$, $\mathbf{W}^k \in \mathbb{R}^{N_{init} \times d_k}$, $\mathbf{W}^v \in \mathbb{R}^{N_{init} \times d_v}$ are learnable parameters. \mathbf{F} and $\mathbf{Fac}^{(0)}$ are the flow matrix and one-hot initial embedding, respectively. g is a linear function that takes \mathbf{F} and $\mathbf{Att}(\mathbf{Fac}^{(l)}, \mathbf{Fac}^{(l)})$ as input. Practically, we find our model works best for g equals to dot product operation.

Our embedding strategy diverges from (Kwon et al., 2021) by intentionally restricting early interaction between facility and location nodes within the attention layer. This distinction arises from our consideration of facility nodes as separate entities from location nodes. Additionally, recognizing that a flow matrix, when paired with different distance matrices, always forms a valid QAP, our focus is on independently learning facility node embeddings and

location nodes embeddings without involving interaction. Experimental results later substantiate the effectiveness of our embedding strategy.

5.2. The Encoder

The encoder comprises L stacked SAWT encoders, and the architecture of a SAWT encoder is illustrated in Figure 2. It takes the concatenation of facility embeddings $\{fac_i\}_{i=1}^n$ and location embeddings $\{loc_i\}_{i=1}^n$ as input, passing through a Multi-Head Solution Aware Attention (SAWT-Att) sub-layer and a feed-forward network sub-layer. Each sub-layer is succeeded by skip connection (He et al., 2016) and layer normalization (Ba et al., 2016), mirroring the original Transformer design. The encoding process is shown in Equation 6.

$$h'_i = \text{LN}(h_i^{(l)} + \mathbf{SAWT}(\mathbf{H}^{(l)}, \mathbf{F}, \mathbf{D}_\sigma)_i),$$

$$h_i^{(l+1)} = \text{LN}(h'_i + \mathbf{FFN}(h'_i)). \quad (6)$$

SAWT-Att. The SAWT-Att aims to utilize the current solution information to enhance the embeddings. SAWT-Att takes the concatenation of facility embeddings and location embeddings, denoted as $\mathbf{H}^{(0)}$ as input. This concatenation is performed based on the current solution σ .

$$\mathbf{H}^{(0)} = [\mathbf{Fac} \parallel \mathbf{Loc}_\sigma] \mathbf{W}^{(0)}, \mathbf{Loc}_\sigma = \mathbf{X}_\sigma \mathbf{Loc}, \quad (7)$$

where \parallel is the concatenation operation, $\mathbf{W}^{(0)} \in \mathbb{R}^{2d \times d}$ is a trainable parameter matrix and \mathbf{X}_σ is the permutation matrix where $\mathbf{X}_{i, \sigma(i)} = 1$ and other elements equal to 0. Following Equation 7, $\mathbf{Loc}_\sigma = (\mathbf{loc}_{\sigma(1)}, \dots, \mathbf{loc}_{\sigma(n)})$. Based on the definition that $\sigma(i)$ assigns fac_i to $loc_{\sigma(i)}$, it is reasonable to concatenate the facility nodes and location nodes in the way presented in Equation 7. Then we compute the solution aware self-attention correlation following the rule below:

$$\mathbf{SAWT-Att}(\mathbf{H}^{(l)}, \mathbf{F}, \mathbf{D}_\sigma) = \mathbf{Att}(\mathbf{H}^{(l)}, \mathbf{H}^{(l)}) \odot \mathbf{M}_\sigma, \quad (8)$$

$$\mathbf{M}_\sigma = \mathbf{F} \odot \mathbf{D}_\sigma, \mathbf{D}_\sigma = \mathbf{X}_\sigma \mathbf{D},$$

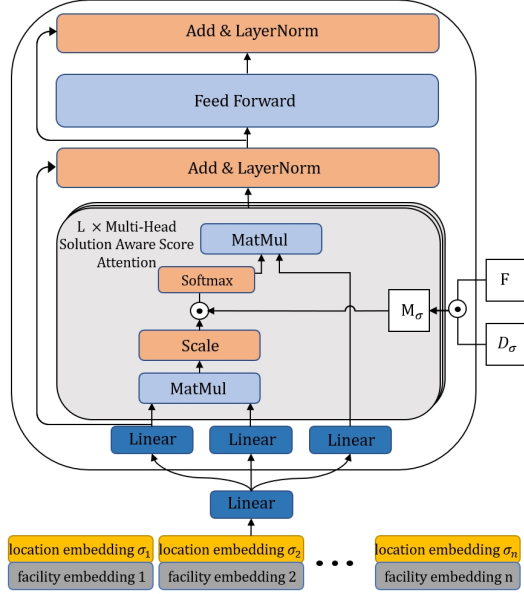


Figure 2. Architecture of SAWT module. For a given current solution σ , we rearrange the rows of the distance matrix to create $\mathbf{D}\sigma = (\mathbf{d}\sigma(1), \dots, \mathbf{d}\sigma(n))$. Conducting a dot product between the flow matrix \mathbf{F} and the distance matrix $\mathbf{D}\sigma$ results in the solution-aware matrix $\mathbf{M}\sigma$, which encapsulates the complete information about the QAP’s objective. This is because the cost for the current solution σ is the sum of $\mathbf{M}\sigma$. By integrating $\mathbf{M}\sigma$ into the attention module, our goal is to equip the model with incumbent solution information.

where \odot is element-wise multiplication.

The self-attention module $\text{Att}(\mathbf{H}^{(l)}, \mathbf{H}^{(l)})$ captures the node-wise relationships within $\mathbf{H}^{(l)}$. The matrix $\mathbf{M}\sigma$, on the other hand, encapsulates the edge-wise relationships present in $\mathbf{H}^{(l)}$. This is evident as $\mathbf{M}\sigma_{\sigma(i), \sigma(j)} = \mathbf{F}_{i,j} \cdot \mathbf{D}_{\sigma(i), \sigma(j)}$ represents the cost associated with assigning facilities i and j to locations $\sigma(i)$ and $\sigma(j)$ respectively. Crucially, $\mathbf{M}\sigma$ is solution-aware, given that $\text{Sum}(\mathbf{M}\sigma) = \text{trace}(\mathbf{F} \cdot \mathbf{X}\sigma \cdot \mathbf{D} \cdot \mathbf{X}\sigma^T)$ from Equation 2 denotes the QAP cost with the solution σ . By combining $\mathbf{M}\sigma$ with self-attention correlation $\text{Att}(\mathbf{H}^{(l)}, \mathbf{H}^{(l)})$, we aim to enhance the model’s ability to capture diverse QAP patterns with different solutions. Importantly, SAWT incorporates the objective gradient information of QAP into its model design for the fact that $\mathbf{M}\sigma \propto D_X \text{trace}(\mathbf{F} \cdot \mathbf{X} \cdot \mathbf{D} \cdot \mathbf{X}^T)$ where details are in Appendix B. This allows $\mathbf{M}\sigma$ to guide the model in the descent direction, leading to improved solutions. Subsequently, the output of SAWT is obtained using a multi-head attention scheme (Vaswani et al., 2017):

$$\begin{aligned} \text{SAWT}(\mathbf{H}^{(l)}, \mathbf{F}, \mathbf{D}\sigma)_i &= \text{Concat}[\text{head}_{i,1}, \dots, \text{head}_{i,m}] \mathbf{W}^O, \\ \text{head}_{i,j} &= (\text{softmax}(\text{SAWT-Att}(\mathbf{H}^{(l)}, \mathbf{F}, \mathbf{D}\sigma)) (\mathbf{H}^{(l)} \mathbf{W}_j^v))_i, \end{aligned} \quad (9)$$

where $\mathbf{W}_j^v \in \mathbb{R}^{d \times d_v}$ and $\mathbf{W}^O \in \mathbb{R}^{md_v \times d}$ are trainable

matrices.

5.3. The Decoder

The decoder processes the SAWT encoder’s output, denoted as $\{h_i^{(L)}\}_{i=1}^n$ and $\{h_i^{*(L)}\}_{i=1}^n$, as input and produces the probability of action pairs $\pi_\theta(A|\bar{\sigma})$ and the value of the current state $V_\phi(\bar{\sigma})$. Each of these components will be explained in detail.

Policy decoder. Our policy decoder primarily comprises a **Max-Pooling** sub-layer and an Action Selection Network (**AS-Net**) sub-layer. In alignment with (Bello et al., 2017), our **AS-Net** employs the chain rule to factorize the probability of swap operations:

$$\pi_\theta(A = (a_1, a_2)|\bar{\sigma}) = p_{\theta_2}(a_2|a_1, \bar{\sigma}) p_{\theta_1}(a_1|\bar{\sigma}), \quad (10)$$

where $\theta = (\theta_1, \theta_2)$ are learnable parameters and $p_{\theta_1}, p_{\theta_2}$ are MLPs followed by a softmax functions elaborated in Equation (11), namely

$$\begin{aligned} p_{\theta_1}(a_1|\bar{\sigma}) &= \text{MLP}_{\theta_1}(h_v^* || \{h_i^{(L)}\}_{i=1}^n), \\ p_{\theta_2}(a_2|a_1, \bar{\sigma}) &= \text{MLP}_{\theta_2}(h_v^* || \{h_i^{(L)}\}_{i=1}^n || h_{a_1}^{(L)}), \end{aligned} \quad (11)$$

where $h_v^* = \mathbf{Max}(\{h_i^{*(L)}\}_{i=1}^n)$ and $\text{MLP}_{\theta_1}, \text{MLP}_{\theta_2}$ consist of three hidden layers each followed by a ReLU activation function. **Max** is the **Max-Pooling** operation that extracts the global representation of the best-found solution σ^* .

Value decoder. Our value decoder aims to evaluate the current state $\bar{\sigma} = (\sigma, \sigma^*)$,

$$V_\phi(\bar{\sigma}) = \mathbf{W}_2 \text{ReLU}(\mathbf{W}_1 (\frac{1}{n} \sum_{i=1}^n h_i^{(L)} + h_v^*) + \mathbf{b}_1) + \mathbf{b}_2, \quad (12)$$

where $\mathbf{W}_1 \in \mathbb{R}^{d \times d}, \mathbf{W}_2 \in \mathbb{R}^{1 \times d}, \mathbf{b}_1 \in \mathbb{R}^d, \mathbf{b}_2 \in \mathbb{R}^1$ are all learnable parameters. We use mean-pooling to represent the global embedding of the solution σ .

5.4. Reinforcement Learning Training Algorithm

We maximize the expected rewards given a state $\bar{\sigma}$, defined as $J(\theta|\bar{\sigma}) = \mathbb{E}\pi_\theta[G_t|\bar{\sigma}]$, through policy gradient optimization, following the approach in (Costa et al., 2020). During training, with a distribution of the state Σ , we optimize the objective function $J(\theta) = \mathbb{E}_{\bar{\sigma} \sim \Sigma}[J(\theta|\bar{\sigma})]$. The training scheme closely resembles REINFORCE (Williams, 1992), and we optimize our policy using the approximate gradient below:

$$\nabla_\theta J(\theta) = \frac{1}{B} \frac{1}{T} \left[\sum_{b=1}^B \sum_{t=0}^{T-1} \nabla_\theta \log(\pi_\theta(A_t^b|\bar{\sigma}_t^b)) (G_t^b - V_\phi(\bar{\sigma}_t^b)) \right], \quad (13)$$

where $G_t^b = \sum_{t'=t}^{T+t-1} \gamma^{t'-t} r^b(t')$. T is the bootstrapping step within an episode.

Table 1. The experiments were conducted on the QAP of sizes 10, 20, 50, and 100. For each size, we trained on 5120 instances with a batch size of 512 and evaluated 256 instances. “MEAN” means the mean cost averaged on the total test instances. “TIME” means the total time needed to solve the test instances. “—” means that the method can not solve the QAP due to the limited CPU memory or GPU memory. “MatNet*” indicates our adoption of the MatNet encoding method to implement an improvement strategy. “**” means that we use 4 CPU units to solve the test instances due to the long inference time.

METHOD	QAP10			QAP20			QAP50			QAP100		
	MEAN↓	GAP↓	TIME↓	MEAN↓	GAP↓	TIME↓	MEAN↓	GAP↓	TIME↓	MEAN↓	GAP↓	TIME↓
GUROBI	11.79	0.00%	5M	55.18	0.45%	1D18H50M	392.57	3.27%	1D18H2M	—	—	—
TS{1K}	11.84	0.42%	2M3S	55.16	0.41%	12M27S	380.56	0.11%	2H27M	1615.77	0.43%	12H32M**
TS{5K}	11.79	0.00%	11M10S	54.93	0.00%	1H38M	380.13	0.00%	17H56M	1608.82	0.00%	6D23H34M**
SM	16.29	38.16%	0.1s	70.07	27.56%	1.1s	446.62	17.49%	18.3s	1800.75	11.92%	3M
RRWM	17.28	46.56%	6.7S	73.74	34.24%	14.3s	457.40	20.32%	39.6s	1823.76	13.36%	4M
IPFP	17.55	48.85%	0.4s	75.52	37.48%	2.4s	479.44	26.12%	47.4s	1911.90	18.83%	5M
MATNET* {10K}	12.67	7.46%	5M12S	61.89	12.67%	17M29S	—	—	—	—	—	—
COSTA {10K}	12.08	2.45%	2M15S	57.91	5.42%	3M15S	404.28	6.35%	5M34s	1720.62	6.94%	9M20s
SUI {10K}	12.04	2.1%	2M25S	56.75	3.32%	3M58S	396.24	4.24%	7M21s	1689.56	5.01%	10M19s
WU {10K}	12.36	4.83%	2M27S	61.24	11.48%	4M35S	425.06	11.81%	9M45S	1766.88	9.82%	13M37s
DACT {10K}	12.30	4.32%	1M59S	60.47	10.08%	2M38S	418.77	10.16%	3M7s	1743.82	8.39%	4M17s
NEUOPT {10K}	12.46	5.68%	3M33S	61.37	11.72%	4M27S	430.61	13.27%	9M23	1789.22	11.21%	14M23s
RGM	12.00	1.78%	51.2s	55.96	1.87%	8M32s	—	—	—	—	—	—
SAWT {2K}	11.87	0.67%	15s	54.97	0.07%	29s	382.36	0.58%	31s	1629.09	1.25%	1M30s
SAWT {4K}	11.84	0.42%	31s	54.80	-0.23%	58s	381.74	0.43%	1M5s	1622.39	0.84%	2M54s
SAWT {10K}	11.79	0.00%	2M30s	54.63	-0.54%	2M32s	379.96	-0.04%	2M40s	1617.23	0.52%	7M32s

To augment the exploration capability of our agent, we include an entropy term the same as (Schulman et al., 2017) and (Costa et al., 2020):

$$H(\theta) = \frac{1}{B} \sum_{b=1}^B \sum_{t=0}^T H(\pi_{\theta}(\cdot | \bar{\sigma}_t^b)), \quad (14)$$

where $H(\pi_{\theta}(\cdot | \bar{\sigma}_t^b)) = -\mathbb{E}_{\pi_{\theta}}[\log \pi_{\theta}(\cdot | \bar{\sigma}_t^b)]$. Finally, we optimize the value function using the loss:

$$\mathcal{L}(\phi) = \frac{1}{B} \sum_{b=1}^B \sum_{t=0}^{T-1} \|G_t^b - V_{\phi}(\bar{\sigma}_t^b)\|_2^2. \quad (15)$$

More architecture details can be found in Appendix A.

6. Experiments

This section details the evaluation setup and presents the results. Additional experiments are provided in Appendix F. The corresponding code and other resources are released at <https://github.com/PKUTAN/SAWT>.

6.1. Experimental Setup

Instance generation. We evaluate our method across four benchmark tasks: Koopmans-Beckmann’s QAP with 10, 20, 50, and 100 nodes, denoted as QAP10, QAP20, QAP50, and QAP100, respectively. In all tasks, location node coordinates are uniformly randomly drawn from the unit square $[0, 1]^2$. The flow f_{ij} from facility i to facility j is sampled uniformly at random from $[0, 1]$ with $f_{ij} = f_{ji}$. We then set the diagonal elements to zero and randomly set $f_{ij} = f_{ji} = 0$ with a probability p . For all experiments, we use a training set of up to 5120 instances and evaluate results on a test set of 256 different instances from the same distribution. We set $p = 0.7$ for all tasks.

QAPLIB Benchmark. The QAPLIB comprises 134 real-world QAP instances spanning 15 categories, such as planning hospital facility layouts. Table 2 displays each category name, like “bur,” along with the instance size indicated within brackets. Each instance comprises a flow matrix and a distance matrix, with different distributions of flow and distance metrics across categories. To ensure a fair comparison, we adhere to the same settings as (Liu et al., 2022). Additional statistical details of QAPLIB can be found in Appendix C.

Baselines. For the self-generated Koopmans-Beckmann’s QAP tasks, we compare our proposed method SAWT with four categories of baselines: (1) **Exact solvers:** Gurobi (Gurobi, 2023) and Tabu-search (TS)(Zhang et al., 2020) (2) **Heuristic solvers:** SM (Leordeanu & Hebert, 2005), RRWM (Cho et al., 2010), and IPFP (Leordeanu et al., 2009). (3) **L2I methods:** MatNet* (Kwon et al., 2021), Costa (Costa et al., 2020), Sui (Sui et al., 2021), Wu (Wu et al., 2021), Dact (Ma et al., 2021), and NeuOpt (Ma et al., 2023). (4) **L2C methods:** RGM (Liu et al., 2022). For QAPLIB benchmarks, following (Liu et al., 2022), the baselines are (1) **Heuristic solvers:** SM, RRWM, and SK-JA (Kushinsky et al., 2019) and (2) **Neural solvers:** NGM (Wang et al., 2021) and RGM (Liu et al., 2022). The baseline details are in Appendix D.

For heuristic solvers, SM, RRWM, and IPFP are renowned for matching problems. For the L2I methods, given the absence of prior work on QAP, we derive baselines from the MILP community, with a particular emphasis on VRPs. As for L2C solvers, RGM is the state-of-the-art RL method for solving QAPLIB. To demonstrate the effectiveness of our model, we slightly adapt the L2I methods to suit QAP by replacing their embeddings with those from our model. It is noteworthy that MatNet, initially an L2C method, is modified into an L2I method, denoted as MatNet*. Detailed

Table 2. Generalization experiments using a policy pre-trained on QAP50, applied to instances from QAPLIB. The mean/max/min gaps are reported for each category. The mean performance over all categories and the inference time (s) per instance are reported.

	BUR (26)			CHR(12-25)			ESC (16-64)			HAD (12 - 20)		
	MEAN↓	MIN↓	MAX↓	MEAN↓	MIN↓	MAX↓	MEAN↓	MIN↓	MAX↓	MEAN↓	MIN↓	MAX↓
SM	22.3	20.3	24.9	460.1	144.6	869.1	301.6	0.0	3300.0	17.4	14.7	21.5
RRWM	23.1	19.3	27.3	616.0	120.5	1346.3	63.9	0.0	200.0	25.1	22.1	28.3
SK-JA	4.7	2.8	6.2	38.5	0.0	186.1	364.8	0.0	2200.0	25.8	6.9	100.0
NGM	3.4	2.8	4.4	121.3	45.4	251.9	126.7	0.0	200.0	8.2	6.0	11.6
RGM	7.1	4.5	9.0	112.4	23.4	361.4	32.8	0.0	141.5	6.2	1.9	9.0
SAWT	2.8	2.2	3.4	110.7	8.6	201.2	13.5	0.0	63.7	3.8	1.6	6.5
	KRA (30-32)			LIPA (20-60)			NUG (12-30)			ROU (12-30)		
	MEAN↓	MIN↓	MAX↓	MEAN↓	MIN↓	MAX↓	MEAN↓	MIN↓	MAX↓	MEAN↓	MIN↓	MAX↓
SM	65.3	63.8	67.3	19.0	3.8	34.8	45.5	34.2	64.0	35.8	30.9	38.2
RRWM	58.8	53.9	67.7	20.9	3.6	41.2	67.8	52.6	79.6	51.2	39.3	60.1
SK-JA	41.4	38.9	44.4	0.0	0.0	0.0	25.3	10.9	100.0	13.7	10.3	17.4
NGM	31.6	28.7	36.8	16.2	3.6	29.4	21.0	14.0	28.5	30.9	23.7	36.3
RGM	15.0	10.4	20.6	13.3	3.0	23.8	9.7	6.1	12.9	13.4	7.1	16.7
SAWT	30.1	28.1	34.2	0.4	0.0	2.6	9.2	4.1	13.1	10.8	8.2	13.1
	SCR (12-20)			SKO(42-64)			STE(36)			TAI(12-64)		
	MEAN↓	MIN↓	MAX↓	MEAN↓	MIN↓	MAX↓	MEAN↓	MIN↓	MAX↓	MEAN↓	MIN↓	MAX↓
SM	123.4	104.0	139.1	29.0	26.6	31.4	475.5	197.7	1013.6	180.5	21.6	1257.9
RRWM	173.5	98.9	218.6	48.5	47.7	49.3	539.4	249.5	1117.8	197.2	26.8	1256.7
SK-JA	48.6	44.3	55.7	18.3	16.1	20.5	120.4	72.5	200.4	25.2	1.6	107.1
NGM	55.5	41.4	66.2	25.2	22.8	27.7	101.7	57.6	172.8	61.4	18.7	352.1
RGM	45.5	30.2	56.1	10.6	9.9	11.2	134.1	69.9	237.0	17.3	11.4	28.6
SAWT	28.5	10.2	48.0	17.7	16.7	18.7	93.5	46.7	170.2	16.5	0.5	48.7
	THO (30-40)			WIL(50)			AVERAGE(12-64)			TIME PER INSTANCE (IN SECONDS)		
	MEAN↓	MIN↓	MAX↓	MEAN↓	MIN↓	MAX↓	MEAN↓	MIN↓	MAX↓			
SM	55.0	54.0	56.0	13.8	11.7	15.9	181.2	46.9	949.9	0.01		
RRWM	80.6	78.2	83.0	18.2	12.5	23.8	169.5	49.5	432.9	0.15		
SK-JA	32.9	30.6	35.3	8.8	6.7	10.7	93.2	9.0	497.9	563.4		
NGM	27.5	24.8	30.2	10.8	8.2	11.1	62.4	17.8	129.7	15.72		
RGM	20.7	12.7	28.6	8.1	7.9	8.4	35.8	10.7	101.1	75.53		
SAWT	24.8	23.2	26.4	8.1	7.6	8.6	26.8	11.2	47.0	12.11		

implementation information can be found in Appendix E.

In contrast to MILP, efficiently solving the QAP to optimality is a challenging task. Despite the rapid optimization capabilities of commercial solvers like Gurobi, SCIP (Bestuzheva et al., 2021), and LKH (Helsgaun, 2017) for MILP, the QAP presents a different scenario. Currently, there is no commercial solver that can efficiently handle the QAP to optimal, even for instances as small as a size of 20. Therefore, as a compromise between performance and efficiency, we have implemented the Tabu-search algorithm (Zhang et al., 2020). We conduct a search step of 5000 to acquire the Best-Known Solution (BKS) for comparative analysis. Specifically, for QAP10, we leverage Gurobi to solve instances optimally. For QAP20 and QAP50, we limit the solution time to 10 minutes per instance. However, when addressing QAP100, Gurobi reported a segmentation fault on our hardware, primarily attributed to constraints in CPU memory capacity.

Metrics. We assess all approaches using two key metrics: (1) The **Mean** objective value, calculated as the average over all test instances using Equation 2. (2) The **Gap**, representing the difference between the **Mean** objective value of the approaches and the **Mean*** objective value of the BKS, defined as $Gap = \frac{Mean - Mean^*}{Mean^*}$.

Implementation. Our model SAWT is implemented using PyTorch (Paszke et al., 2019). All experiments are executed

on a single NVIDIA 3080Ti GPU (12GB) and a 12th Gen Intel(R) Core(TM) i5-12600KF 3.69 GHz CPU. We train the model for 200 epochs with a batch size of 512 and an episode length of 400 for all tasks. Each epoch requires an average time of 1m40s, 4m20s, 9m54s, and 19m48s for QAP10, QAP20, QAP50, and QAP100, respectively. During testing, our policy runs for 2000, 4000, and 10000 steps on 256 instances, and we use the averaged objective value for comparison with other baselines.

6.2. Experimental Results

Results on Koopmans-Beckmann’s QAP. Table 1 presents the results for Koopmans-Beckmann’s QAP. It is evident that QAP10 is relatively straightforward, with Gurobi achieving optimal solutions for all 256 testing instances within 5 minutes. However, Gurobi faces significant challenges with QAP100, reaching the limits of CPU memory capacity. These Gurobi-based outcomes underscore the inherent complexities associated with solving the QAP. Additionally, the performance issues encountered by all three heuristics further emphasize the difficulty of QAP.

Regarding the L2I methods, there are three main observations: (1) All L2I methods exhibit poor performance. The best gaps on four tasks are 2.1%, 3.32%, 4.24%, and 5.01% which are almost an average of $10 \times$ larger than the gaps achieved by our SAWT method at the 2000-step search. This

Table 3. Generalization to different sizes of the QAP instances.

METHODS	QAP20	QAP50	QAP100
POLICY-20	54.63	383.67	1641.40
POLICY-50	54.78	380.38	1617.84
POLICY-100	54.82	381.13	1617.23

is because they are designed to capture the linear structure of the VRPs that can not learn the higher-order patterns in the QAPs. (2) MatNet* displays notably poor performance, significantly trailing our SAWT by margins of 0.67% and 0.07% even with a search step of 2000. This suggests the effectiveness of our SAWT to encode the facility and location nodes independently. Furthermore, the dual attention structure of MatNet* leads to high computational complexity, resulting in its inability to solve larger instances like QAP50 and QAP100. (3) Our SAWT model demonstrates superior performance over all heuristic and L2I baselines, even with a search step constraint of 2000, showing a strong ability to learn the patterns of the QAP. This leads to even smaller gaps of 0.00% (QAP10), -0.45% (QAP20), -0.04% (QAP50), and 0.52% (QAP100) when the search step is increased to 10,000.

In L2C methods, RGM outperforms all L2I methods on QAP10 and QAP20, achieving gaps of 1.78% and 1.87%, respectively. This success stems from RGM’s learning strategy, enabling it to grasp more complex patterns within the QAP. However, severe scalability issues plague RGM, making it incapable of solving QAP instances beyond a size of 50. This substantial limitation, arising from constraints associated with the association graph, severely restricts RGM’s potential for real-world applications.

In terms of inference time, our SAWT model demonstrates comparable efficiency to Dact and slightly outperforms other L2I methods. Notably, with a search step of 10,000, our model achieves significantly faster inference times than the exact solver Tabu-search with a step size of 5,000. Specifically, it is 4.7× faster for QAP10, 38.7× for QAP20, 403× for QAP50, and an impressive 5350× faster for QAP100. In summary, our SAWT model excels in both effectiveness and efficiency when solving the QAP.

Generalization to Different Sizes. We evaluate the performance of our policies trained on QAP20, QAP50, and QAP100 when applied to QAP tasks of varying sizes. Since our facility nodes embedding design, as outlined in section 5.1, adopt a strategy of randomly choosing a N_{init} -dimensional one-hot vector for the initial embeddings, we can develop generalized policies capable of solving the QAP for any instance with a size less than N_{init} , we set $N_{init} = 128$ for our experiments. As depicted in Table 3, all our policies demonstrate the ability to generalize effectively across different task sizes. Among all, Policy-50 exhibits superior generalization compared to other policies. Surpass-

Table 4. Ablation studies on 256 QAP20 instances running policies for 10000 steps.

SINGLE-AM	SAWT-ENCODER	MEAN	GAP
×	×	62.38	13.56%
×	✓	61.89	12.67%
✓	×	57.00	3.76%
✓	✓	54.63	-0.54%

ing Policy-100 in QAP20 performance with a score of 54.78 versus 54.82, Policy-50 maintains competitive effectiveness on QAP100, achieving a score of 1617.84 against 1617.23, reflecting a marginal difference of only 0.03%.

Generalization to QAPLIB. We extend our experiments to evaluate the SAWT model on the QAPLIB benchmark, utilizing Policy-50 for solving instances from QAPLIB. The results, summarized in Table 2, show our model’s superiority, surpassing all baseline metrics with an average mean of 26.8% and a maximum value of 47.0%. Additionally, our model outperforms learning methods such as RGM and NGM in terms of inference speed. Noteworthy observations from Table 2 reveal that while the SAWT method excels in performance on datasets like “Bur” and “Lipa,” it faces challenges on datasets such as “Chr” and “Ste,” evidenced by substantial Mean gaps of 110.7% and 93.5%. This performance variation can be attributed to specific dataset characteristics, including the extreme sparsity of the flow matrix in “Chr” and the distance matrix in “Ste,” resulting in a significant distribution shift compared to our training dataset. Further details on QAPLIB experiments are available in Appendix F.5.

6.3. Additional Analysis

Ablation studies. In Table 4, we present an ablation study of the proposed method: SAWT. “Single-AM” implies that we only use a single self-attention model and a GCN to encode the facility and location nodes, which is aligned with our formal design, otherwise, we use a dual self-attention method as in MatNet. As shown in the table, both “Single-AM” and “SAWT-encoder” play an important role in our model. Without “Single-AM”, the model struggles to tackle the QAP, this proves the fact that we need to process facility and location nodes differently without early interaction as they are from different domains. “SAWT-encoder” is also indispensable, by equipping our model with “SAWT-encoder”, the gaps lowered from 13.56% to 11.94% and from 3.78% to -0.45%. In conclusion, we consider “Single-AM” to be more crucial than “SAWT-encoder” in our model. This is because without meaningful representations, the model faces significant challenges in effectively solving the QAP.

Robustness against initial solution. In Tables 5 and 6, we assess our model’s robustness against random initial solu-

Table 5. Random initial solutions experiments on QAP tasks.

METHODS	QAP20		QAP50		QAP100	
	MEAN	GAP	MEAN	GAP	MEAN	GAP
SAWT	54.63 \pm 0.00	-0.54% \pm 0.01	379.97 \pm 0.12	-0.04% \pm 0.03	1617.08 \pm 2.84	0.51% \pm 0.12
SAWT(RAND)	54.69 \pm 0.02	-0.43% \pm 0.03	380.83 \pm 0.72	0.18% \pm 0.18	1622.06 \pm 4.21	0.82% \pm 0.26
SAWT-RAND	54.62 \pm 0.00	-0.55% \pm 0.03	379.35 \pm 0.06	-0.38% \pm 0.01	1614.42 \pm 1.03	0.34% \pm 0.07

Table 6. Random initial solutions experiments on QAPLIB.

	BUR	CHR	ESC	HAD	KRA	LIPA	NUG
SAWT	2.8% \pm 0.0	108.6% \pm 8.2	14.2% \pm 1.4	3.7% \pm 0.2	31.2% \pm 1.7	0.4% \pm 0.0	9.1% \pm 0.2
SAWT(RAND)	3.3% \pm 0.3	128.2% \pm 29.4	13.1% \pm 2.1	4.5% \pm 0.5	42.2% \pm 14.2	0.7% \pm 0.2	11.3% \pm 1.9
SAWT-RAND	2.6% \pm 0.1	84.6% \pm 3.1	12.9% \pm 0.6	3.4% \pm 0.3	28.7% \pm 1.4	0.4% \pm 0.1	9.0% \pm 0.3
	ROU	SCR	SKO	STE	TAI	THO	WIL
SAWT	10.5% \pm 0.5	29.0% \pm 1.1	17.7% \pm 0.9	98.2% \pm 5.1	16.3% \pm 0.3	24.3% \pm 1.1	8.1 \pm 0.5
SAWT(RAND)	9.2% \pm 1.7	32.8% \pm 4.4	15.3% \pm 5.3	124.5% \pm 20.7	16.4% \pm 0.8	24.1% \pm 2.3	10.3 \pm 2.6
SAWT-RAND	8.5% \pm 0.9	29.5% \pm 2.4	13.4% \pm 0.7	75.6% \pm 9.5	16.0% \pm 0.4	20.2% \pm 1.2	7.9% \pm 0.9

tions for QAP tasks and QAPLIB. “SAWT (RAND)” refers to SAWT trained with a fixed initial solution but evaluated with random ones, while “SAWT-RAND” is both trained and evaluated with random initial solutions. Two key observations emerge: (1) SAWT (RAND) performs the worst, and SAWT-RAND the best, for both QAP tasks and QAPLIB. This can be attributed to the “explore and exploit” principle of RL. By using diverse initial solutions, SAWT-RAND effectively explores the solution space, thereby improving its performance. (2) The variance in Table 6 for SAWT-RAND is generally lower than for SAWT (RAND) but higher than for SAWT. This results from their initial solution strategies: SAWT uses fixed initial solutions, while both SAWT-RAND and SAWT (RAND) use random ones. In summary, SAWT-RAND demonstrates superior performance on both QAP tasks and QAPLIB, highlighting our model’s robustness against random initial solutions.

7. Conclusions

In this paper, we introduce SAWT, a novel L2I solver for Koopmans-Beckmann’s QAP, the first L2I method to solve the complex QAP. It first processes the facility and location nodes independently by a self-attention model and a GCN. It is then followed by an SAWT encoder to capture the rich patterns in QAP. Extensive experiments on both synthetic and benchmark datasets justified the effectiveness of SAWT in terms of both inference and generalization. Additional analysis furthermore demonstrates the robustness of SAWT. It is future work to learn a model that has stronger generalization ability. Although SAWT achieves the best performance on the QAPLIB, it still has a relatively high mean gap. This is mainly because of the diverse distribution of instances in the QAPLIB. In the future, it is desirable to utilize a meta-learning strategy to enhance SAWT, so that it can perform better on QAPLIB.

Acknowledgement

This research work is supported by National Key R&D Program of China (2022ZD0160305), a research grant from China Tower Corporation Limited, and a grant from Beijing Aerospace Automatic Control Institute.

Impact Statement

This work boosts the scalability, performance, and efficiency of solving QAPs but necessitates vigilant data safety measures due to its wide real-world applicability in areas such as chip placement and hospital layouts. The risk of data leakage looms, particularly with sensitive datasets like chip circuits or confidential hospital patient data. Currently, as we focus on learning-based methods with self-generated tasks, data safety concerns are not immediate. However, the future potential for data safety issues warrants attention.

References

- Ahmed, Z. H. A multi-parent genetic algorithm for the quadratic assignment problem. *Opsearch*, 52:714–732, 2015.
- Ahn, S., Kim, J., Lee, H., and Shin, J. Guiding deep molecular optimization with genetic exploration. In Larochelle, H., Ranzato, M., Hadsell, R., Balcan, M., and Lin, H. (eds.), *Advances in Neural Information Processing Systems 33: Annual Conference on Neural Information Processing Systems 2020, NeurIPS 2020, December 6-12, 2020, virtual*, 2020.
- Ba, L. J., Kiros, J. R., and Hinton, G. E. Layer normalization. *CoRR*, abs/1607.06450, 2016.
- Bello, I., Pham, H., Le, Q. V., Norouzi, M., and Bengio, S. Neural combinatorial optimization with reinforcement learning. In *5th International Conference on Learning Representations, ICLR 2017, Toulon, France, April 24-*

- 26, 2017, *Workshop Track Proceedings*. OpenReview.net, 2017.
- Bestuzheva, K., Besançon, M., Chen, W.-K., Chmiela, A., Donkiewicz, T., van Doornmalen, J., Eifler, L., Gaul, O., Gamrath, G., Gleixner, A., et al. The scip optimization suite 8.0. *arXiv preprint arXiv:2112.08872*, 2021.
- Burkard, R. E., Karisch, S. E., and Rendl, F. Qaplib—a quadratic assignment problem library. *Journal of Global optimization*, 10:391–403, 1997.
- Chen, X. and Tian, Y. Learning to perform local rewriting for combinatorial optimization. *Advances in Neural Information Processing Systems*, 32, 2019.
- Cho, M., Lee, J., and Lee, K. M. Reweighted random walks for graph matching. In *Computer Vision—ECCV 2010: 11th European Conference on Computer Vision, Heraklion, Crete, Greece, September 5–11, 2010, Proceedings, Part V 11*, pp. 492–505. Springer, 2010.
- Costa, P. R., Rhuggenaath, J., Zhang, Y., and Akcay, A. Learning 2-opt heuristics for the traveling salesman problem via deep reinforcement learning. In *Asian conference on machine learning*, pp. 465–480. PMLR, 2020.
- Cui, K., Baumgärtner, L., Yilmaz, M. B., Li, M., Fabian, C., Becker, B., Xiang, L., Bauer, M., and Koeppl, H. Uav swarms for joint data ferrying and dynamic cell coverage via optimal transport descent and quadratic assignment. In *2023 IEEE 48th Conference on Local Computer Networks (LCN)*, pp. 1–8. IEEE, 2023.
- Dai, H., Dai, B., and Song, L. Discriminative embeddings of latent variable models for structured data. In *International conference on machine learning*, pp. 2702–2711. PMLR, 2016.
- Edwards, C. A branch and bound algorithm for the koopmans-beckmann quadratic assignment problem. *Combinatorial optimization II*, pp. 35–52, 1980.
- Elshafei, A. N. Hospital layout as a quadratic assignment problem. *Journal of the Operational Research Society*, 28(1):167–179, 1977.
- Gurobi, L. Gurobi optimizer reference manual, 2023.
- Hanh, N. T., Binh, H. T. T., Hoai, N. X., and Palaniswami, M. S. An efficient genetic algorithm for maximizing area coverage in wireless sensor networks. *Information Sciences*, 488:58–75, 2019.
- He, K., Zhang, X., Ren, S., and Sun, J. Deep residual learning for image recognition. In *2016 IEEE Conference on Computer Vision and Pattern Recognition, CVPR 2016, Las Vegas, NV, USA, June 27–30, 2016*, pp. 770–778. IEEE Computer Society, 2016. doi: 10.1109/CVPR.2016.90.
- Helsgaun, K. Lkh-3 version 3.0. 6 (may 2019), 2017.
- Hu, Z., Sun, Y., and Yang, Y. Switch to generalize: Domain-switch learning for cross-domain few-shot classification. In *International Conference on Learning Representations*, 2022. URL <https://openreview.net/forum?id=H-iABMvzIc>.
- Hu, Z., Sun, Y., Wang, J., and Yang, Y. DAC-DETR: Divide the attention layers and conquer. In *Thirty-seventh Conference on Neural Information Processing Systems*, 2023a. URL <https://openreview.net/forum?id=8JMexYVcXB>.
- Hu, Z., Sun, Y., and Yang, Y. Suppressing the heterogeneity: A strong feature extractor for few-shot segmentation. In *The Eleventh International Conference on Learning Representations*, 2023b. URL <https://openreview.net/forum?id=CGUvK3U09LH>.
- James, T., Rego, C., and Glover, F. A cooperative parallel tabu search algorithm for the quadratic assignment problem. *European Journal of Operational Research*, 195(3): 810–826, 2009.
- Jiang, B., Jin, Y., Tan, Z., and Mu, Y. Video action segmentation via contextually refined temporal keypoints. In *Proceedings of the IEEE/CVF International Conference on Computer Vision*, pp. 13836–13845, 2023.
- Khalil, E., Dai, H., Zhang, Y., Dilkina, B., and Song, L. Learning combinatorial optimization algorithms over graphs. *Advances in neural information processing systems*, 30, 2017.
- Koopmans, T. C. and Beckmann, M. Assignment problems and the location of economic activities. *Econometrica: journal of the Econometric Society*, pp. 53–76, 1957.
- Kushinsky, Y., Maron, H., Dym, N., and Lipman, Y. Sinkhorn algorithm for lifted assignment problems. *SIAM Journal on Imaging Sciences*, 12(2):716–735, 2019.
- Kwon, Y., Choo, J., Yoon, I., Park, M., Park, D., and Gwon, Y. Matrix encoding networks for neural combinatorial optimization. In Ranzato, M., Beygelzimer, A., Dauphin, Y. N., Liang, P., and Vaughan, J. W. (eds.), *Advances in Neural Information Processing Systems 34: Annual Conference on Neural Information Processing Systems 2021, NeurIPS 2021, December 6–14, 2021, virtual*, pp. 5138–5149, 2021.
- Kwon, Y.-D., Choo, J., Kim, B., Yoon, I., Gwon, Y., and Min, S. Pomo: Policy optimization with multiple optima for reinforcement learning. *Advances in Neural Information Processing Systems*, 33:21188–21198, 2020.

- Lai, Y., Mu, Y., and Luo, P. Maskplace: Fast chip placement via reinforced visual representation learning. In Koyejo, S., Mohamed, S., Agarwal, A., Belgrave, D., Cho, K., and Oh, A. (eds.), *Advances in Neural Information Processing Systems 35: Annual Conference on Neural Information Processing Systems 2022, NeurIPS 2022, New Orleans, LA, USA, November 28 - December 9, 2022*, 2022.
- Laporte, G. and Mercure, H. Balancing hydraulic turbine runners: A quadratic assignment problem. *European Journal of Operational Research*, 35(3):378–381, 1988. ISSN 0377-2217. doi: [https://doi.org/10.1016/0377-2217\(88\)90227-5](https://doi.org/10.1016/0377-2217(88)90227-5).
- Leordeanu, M. and Hebert, M. A spectral technique for correspondence problems using pairwise constraints. In *Tenth IEEE International Conference on Computer Vision (ICCV'05) Volume 1*, volume 2, pp. 1482–1489. IEEE, 2005.
- Leordeanu, M., Hebert, M., and Sukthankar, R. An integer projected fixed point method for graph matching and map inference. *Advances in neural information processing systems*, 22, 2009.
- Lin, Y., Yang, M., Yu, J., Hu, P., Zhang, C., and Peng, X. Graph matching with bi-level noisy correspondence. In *Proceedings of the IEEE/CVF International Conference on Computer Vision*, pp. 23362–23371, 2023.
- Liu, C., Jiang, Z., Wang, R., Huang, L., Lu, P., and Yan, J. Revocable deep reinforcement learning with affinity regularization for outlier-robust graph matching. In *The Eleventh International Conference on Learning Representations*, 2022.
- Ma, Y., Li, J., Cao, Z., Song, W., Zhang, L., Chen, Z., and Tang, J. Learning to iteratively solve routing problems with dual-aspect collaborative transformer. *Advances in Neural Information Processing Systems*, 34:11096–11107, 2021.
- Ma, Y., Cao, Z., and Chee, Y. M. Learning to search feasible and infeasible regions of routing problems with flexible neural k-opt. *arXiv preprint arXiv:2310.18264*, 2023.
- Mihić, K., Ryan, K., and Wood, A. Randomized decomposition solver with the quadratic assignment problem as a case study. *INFORMS Journal on Computing*, 30(2): 295–308, 2018.
- Mirhoseini, A., Goldie, A., Yazgan, M., Jiang, J. W., Songhori, E. M., Wang, S., Lee, Y., Johnson, E., Pathak, O., Nazi, A., Pak, J., Tong, A., Srinivasa, K., Hang, W., Tuncer, E., Le, Q. V., Laudon, J., Ho, R., Carpenter, R., and Dean, J. A graph placement methodology for fast chip design. *Nat.*, 594(7862):207–212, 2021. doi: 10.1038/S41586-021-03544-W.
- Nowak, A., Villar, S., Bandeira, A. S., and Bruna, J. Revised note on learning quadratic assignment with graph neural networks. In *2018 IEEE Data Science Workshop (DSW)*, pp. 1–5. IEEE, 2018.
- Paszke, A., Gross, S., Massa, F., Lerer, A., Bradbury, J., Chanan, G., Killeen, T., Lin, Z., Gimelshein, N., Antiga, L., et al. Pytorch: An imperative style, high-performance deep learning library. *Advances in neural information processing systems*, 32, 2019.
- Sahni, S. and Gonzalez, T. F. P-complete approximation problems. *J. ACM*, 23(3):555–565, 1976. doi: 10.1145/321958.321975.
- Schulman, J., Wolski, F., Dhariwal, P., Radford, A., and Klimov, O. Proximal policy optimization algorithms. *CoRR*, abs/1707.06347, 2017.
- Shylo, P. Solving the quadratic assignment problem by the repeated iterated tabu search method. *Cybernetics and Systems Analysis*, 53:308–311, 2017.
- Steinberg, L. The backboard wiring problem: A placement algorithm. *SIAM Review*, 3(1):37–50, 1961. ISSN 00361445.
- Sui, J., Ding, S., Liu, R., Xu, L., and Bu, D. Learning 3-opt heuristics for traveling salesman problem via deep reinforcement learning. In *Asian Conference on Machine Learning*, pp. 1301–1316. PMLR, 2021.
- Taillard, É. Robust taboo search for the quadratic assignment problem. *Parallel computing*, 17(4-5):443–455, 1991.
- Tan, Z. and Mu, Y. Hierarchical reinforcement learning for chip-macro placement in integrated circuit. *Pattern Recognition Letters*, 2024.
- Tan, Z., Wang, W., and Shan, C. Vision transformers are active learners for image copy detection. *Neurocomputing*, 587:127687, 2024.
- Vaswani, A., Shazeer, N., Parmar, N., Uszkoreit, J., Jones, L., Gomez, A. N., Kaiser, L., and Polosukhin, I. Attention is all you need. In Guyon, I., von Luxburg, U., Bengio, S., Wallach, H. M., Fergus, R., Vishwanathan, S. V. N., and Garnett, R. (eds.), *Advances in Neural Information Processing Systems 30: Annual Conference on Neural Information Processing Systems 2017, December 4-9, 2017, Long Beach, CA, USA*, pp. 5998–6008, 2017.
- Veres, M. and Moussa, M. Deep learning for intelligent transportation systems: A survey of emerging trends. *IEEE Trans. Intell. Transp. Syst.*, 21(8):3152–3168, 2020. doi: 10.1109/TITS.2019.2929020.

- Vinyals, O., Fortunato, M., and Jaitly, N. Pointer networks. *Advances in neural information processing systems*, 28, 2015.
- Wang, H. and Alidaee, B. A new hybrid-heuristic for large-scale combinatorial optimization: A case of quadratic assignment problem. *Computers & Industrial Engineering*, 179:109220, 2023.
- Wang, R., Yan, J., and Yang, X. Neural graph matching network: Learning lawler’s quadratic assignment problem with extension to hypergraph and multiple-graph matching. *IEEE Transactions on Pattern Analysis and Machine Intelligence*, 44(9):5261–5279, 2021.
- Williams, R. J. Simple statistical gradient-following algorithms for connectionist reinforcement learning. *Mach. Learn.*, 8:229–256, 1992. doi: 10.1007/BF00992696.
- Wu, Y., Song, W., Cao, Z., Zhang, J., and Lim, A. Learning improvement heuristics for solving routing problems. *IEEE transactions on neural networks and learning systems*, 33(9):5057–5069, 2021.
- Yang, N., Zeng, K., Wu, Q., and Yan, J. Molerec: Combinatorial drug recommendation with substructure-aware molecular representation learning. In Ding, Y., Tang, J., Sequeda, J. F., Aroyo, L., Castillo, C., and Houben, G. (eds.), *Proceedings of the ACM Web Conference 2023, WWW 2023, Austin, TX, USA, 30 April 2023 - 4 May 2023*, pp. 4075–4085. ACM, 2023. doi: 10.1145/3543507.3583872.
- Yu, T., Wang, R., Yan, J., and Li, B. Deep latent graph matching. In *International Conference on Machine Learning*, pp. 12187–12197. PMLR, 2021.
- Zanfir, A. and Sminchisescu, C. Deep learning of graph matching. In *2018 IEEE Conference on Computer Vision and Pattern Recognition, CVPR 2018, Salt Lake City, UT, USA, June 18-22, 2018*, pp. 2684–2693. Computer Vision Foundation / IEEE Computer Society, 2018. doi: 10.1109/CVPR.2018.00284.
- Zhang, H., Liu, F., Zhou, Y., and Zhang, Z. A hybrid method integrating an elite genetic algorithm with tabu search for the quadratic assignment problem. *Information Sciences*, 539:347–374, 2020.
- Zhang, J., Liu, C., Li, X., Zhen, H., Yuan, M., Li, Y., and Yan, J. A survey for solving mixed integer programming via machine learning. *Neurocomputing*, 519:205–217, 2023. doi: 10.1016/J.NEUCOM.2022.11.024.

APPENDIX

A. Network details

Our SAWT model consists of an encoder and a decoder. At first, we initialize the facility nodes with vectors randomly sampled from a one-hot vector pool with a dimension of $N_{init} = 128$. Details are shown below in Python code.

```

1  f_init_emb = torch.zeros(size=(batch_size, node_cnt, N_{init})).to(device)
2  # shape: (batch, node, embedding)
3
4  seed_cnt = 100
5  rand = torch.rand(batch_size, seed_cnt)
6  # Create a random one-hot vector pool for each instance within a batch
7
8  batch_rand_perm = rand.argsort(dim=1)
9  rand_idx = batch_rand_perm[:, :node_cnt]
10 # Collect one-hot vector index for facility nodes, ``node_cnt" refers to the problem
    size
11
12
13 b_idx = torch.arange(batch_size)[:, None].expand(batch_size, node_cnt)
14 n_idx = torch.arange(node_cnt)[None, :].expand(batch_size, node_cnt)
15 f_init_emb[b_idx, n_idx, rand_idx] = 1
16 # Create the one-hot vector
    
```

In our model, facility and location nodes are first processed through a linear function, producing outputs of dimension d_{emb} . We utilize a single-mixed-score Transformer with two modules, each featuring eight heads, alongside a three-layer Graph Convolution Network (GCN), each layer having a hidden dimension of d_{hidden} . The facility and location node representations are then merged and processed through L modules of the SAWT Transformer, maintaining the eight-head configuration. The SAWT Transformer’s output feeds into both policy and value decoders. The policy decoder consists of two Multi-Layer Perceptrons (MLPs): the first, MLP_1 , with three layers sized $(2 \times d_{hidden}, d_{hidden})$, (d_{hidden}, d_{hidden}) , and $(d_{hidden}, 1)$, and the second, MLP_2 , also with three layers but sized $(3 \times d_{hidden}, d_{hidden})$, (d_{hidden}, d_{hidden}) , and $(d_{hidden}, 1)$. These MLPs aim to select a pair of positions for swap operations to generate a new solution state σ' . Meanwhile, the value decoder evaluates the current and optimal solutions (σ, σ^*) to produce a scalar value.

The training parameters in our model are updated using the loss function below:

$$\mathcal{L} = -J(\theta) + 0.99^{epoch} \beta H(\theta) + \zeta \mathcal{L}(\phi). \quad (16)$$

The definitions of $J(\theta)$, $H(\theta)$, and $\mathcal{L}(\phi)$ are provided in Subsection 5.4. The hyper-parameters β and ζ are set to 0.005 and 0.5, respectively, for all experiments. The term 0.99^{epoch} is used to shift the model’s focus towards exploitation in the later training stages. Our policy training closely follows the REINFORCE algorithm, with bootstrapping steps $T = 8$ and a discount factor $\gamma = 0.99$ as detailed in Subsection 5.4. Training includes a total of 400 search steps. The Adam optimizer is employed for gradient updates. Table 7 below summarizes the hyper-parameter settings:

Table 7. Hyperparameter values for each task.

HYPERPARAMETER	QAP10	QAP20	QAP50	QAP100
d_{emb}	64	64	64	64
d_{hidden}	64	64	64	64
L	3	2	3	3
lr	10^{-3}	10^{-3}	10^{-3}	10^{-3}

B. Theoretical insight

The goal of the Quadratic Assignment Problem (QAP) is to minimize the following equation:

$$\min_{\mathbf{X}} \text{trace}(\mathbf{F} \cdot \mathbf{X} \cdot \mathbf{D} \cdot \mathbf{X}^T), \quad (17)$$

$$s.t. \quad \mathbf{X} \cdot \mathbf{1} = \mathbf{1}, \quad (18)$$

$$\mathbf{X}^T \cdot \mathbf{1} = \mathbf{1}, \quad (19)$$

$$\mathbf{X} \in \{0, 1\}^{n \times n}. \quad (20)$$

The gradient of the objective function in any direction represented by matrix \mathbf{V} is given by:

$$\begin{aligned} & \langle D_X \text{trace}(\mathbf{F} \cdot \mathbf{X} \cdot \mathbf{D} \cdot \mathbf{X}^T), \mathbf{V} \rangle \\ &= \langle D_X \text{trace}(\mathbf{X} \cdot \mathbf{D}^T \cdot \mathbf{X}^T \cdot \mathbf{F}^T), \mathbf{V} \rangle \\ &= \lim_{t \rightarrow 0} \frac{\text{trace}((\mathbf{X} + t\mathbf{V}) \cdot \mathbf{D}^T \cdot (\mathbf{X} + t\mathbf{V})^T \cdot \mathbf{F}^T) - \text{trace}(\mathbf{X} \cdot \mathbf{D}^T \cdot \mathbf{X}^T \cdot \mathbf{F}^T)}{t} \\ &= \lim_{t \rightarrow 0} \frac{t^2 \cdot \text{trace}(\mathbf{V} \cdot \mathbf{D}^T \cdot \mathbf{V}^T \cdot \mathbf{F}^T) + t \cdot (\text{trace}(\mathbf{X} \cdot \mathbf{D}^T \cdot \mathbf{V}^T \cdot \mathbf{F}^T) + \text{trace}(\mathbf{V} \cdot \mathbf{D}^T \cdot \mathbf{X}^T \cdot \mathbf{F}^T))}{t} \\ &= \text{trace}(\mathbf{X} \cdot \mathbf{D}^T \cdot \mathbf{V}^T \cdot \mathbf{F}^T) + \text{trace}(\mathbf{V} \cdot \mathbf{D}^T \cdot \mathbf{X}^T \cdot \mathbf{F}^T) \\ &= \text{trace}(\mathbf{F}^T \cdot \mathbf{X} \cdot \mathbf{D}^T \cdot \mathbf{V}^T) + \text{trace}(\mathbf{F} \cdot \mathbf{X} \cdot \mathbf{D} \cdot \mathbf{V}^T) \\ &= \langle \mathbf{F}^T \cdot \mathbf{X} \cdot \mathbf{D}^T, \mathbf{V} \rangle + \langle \mathbf{F} \cdot \mathbf{X} \cdot \mathbf{D}, \mathbf{V} \rangle \\ &= \langle \mathbf{F}^T \cdot \mathbf{X} \cdot \mathbf{D}^T + \mathbf{F} \cdot \mathbf{X} \cdot \mathbf{D}, \mathbf{V} \rangle. \end{aligned} \quad (21)$$

Following our derivation, we find $D_X \text{trace}(\mathbf{F} \cdot \mathbf{X} \cdot \mathbf{D} \cdot \mathbf{X}^T) = \mathbf{F}^T \cdot \mathbf{X} \cdot \mathbf{D}^T + \mathbf{F} \cdot \mathbf{X} \cdot \mathbf{D}$. In our self-generated datasets, where $\mathbf{F} = \mathbf{F}^T$ and $\mathbf{D} = \mathbf{D}^T$, this simplifies to: $D_X \text{trace}(\mathbf{F} \cdot \mathbf{X} \cdot \mathbf{D} \cdot \mathbf{X}^T) = 2 \cdot \mathbf{F} \cdot \mathbf{X} \cdot \mathbf{D}$. This expression matches matrix \mathbf{M} from Equation 8 in our main paper, which is used in the Solution Aware Transformer. We propose that the Solution Aware Transformer’s design, incorporating the objective gradient into the attention layer, aids in pattern learning for QAPs. By applying Equation 13 from our main paper, the reinforcement learning update gradient can be steered correctly, thereby enhancing performance.

C. QAPLIB benchmarks

The QAPLIB¹ (Burkard et al., 1997) includes 134 real-world QAP instances across 15 categories, such as planning and hospital facility layout (Elshafei, 1977), with problem sizes ranging from 12 to 256. Instances are named based on a specific rule: the prefix denotes the problem category (usually the author’s name), followed by a number indicating the problem size. If multiple problems share the same size, a letter starting from *a* is added for distinction. For example, see Equation 22.

$$\frac{\text{bur}}{\text{author name}} - \frac{26}{\text{problem size}} - \frac{a}{\text{index}}. \quad (22)$$

D. Baseline details

We provide detailed information about the methods used in our experiments. Gurobi and TS are exact solvers that perform exhaustive searches for solutions. SM, RRWM, IPFP, and Sinkhorn-JA are heuristics that efficiently handle Lawler’s QAPs

¹<https://coral.ise.lehigh.edu/data-sets/qaplib/>

as shown in Equation 23:

$$\begin{aligned}
 \min_{\mathbf{X}} \quad & \text{vec}(\mathbf{X}) \cdot \mathbf{K} \cdot \text{vec}(\mathbf{X})^T, \\
 \text{s.t.} \quad & \mathbf{X} \cdot \mathbf{1} = \mathbf{1}, \mathbf{X}^T \cdot \mathbf{1} = \mathbf{1}, \\
 & \mathbf{X} \in \{0, 1\}^{n \times n}.
 \end{aligned} \tag{23}$$

The association graph $\mathbf{K} \in \mathbb{R}^{n^2 \times n^2}$ is central to various optimization problems. MatNet is an L2C method designed for solving asymmetric TSPs and flexible flow shop problems. In contrast, Costa, Sui, Wu, Dact, and NeuOpt are L2I methods that address VRPs. Additionally, NGM and RGM are learning-based approaches for solving Lawler’s QAPs.

Gurobi (Gurobi, 2023) is a leading optimization solver, particularly effective in solving combinatorial optimization problems (COPs). It primarily uses the Branch-and-Bound method to perform exhaustive solution searches.

TS (Zhang et al., 2020) This approach integrates a genetic method into tabu-search algorithms. In each iteration, the genetic method selects an elite solution for the tabu list using crossover and mutation processes. The tabu-search algorithm follows the pseudocode from (Zhang et al., 2020).

SM (Leordeanu & Hebert, 2005) considers matching problems as identifying graph clusters in the association graph using traditional spectral techniques. The concept is that nodes to be matched should cluster together.

RRWM (Cho et al., 2010) adopts a reweighted random-walk algorithm on the association graph to solve matching problems.

IPFP (Leordeanu et al., 2009) refines the solution iteratively through integer projection.

SK-JA (Kushinsky et al., 2019) utilizes the widely recognized Johnson–Adams (JA) relaxation, a linear program relaxation of the Quadratic Assignment Problem, to solve instances from QAPLIB.

MatNet* (Kwon et al., 2021) is modified from MatNet, an L2C method that directly encodes matrix inputs. MatNet employs a dual-mixed attention model to integrate the matrix input into the attention mechanism.

Costa (Costa et al., 2020) The model employs an RNN to capture the sequence in TSP solutions. Its decoder utilizes a pointer network to select two locations for a 2-opt operation.

Sui (Sui et al., 2021) It employs a 3-opt heuristic for TSPs, utilizing a link selection network to create fresh connections among the selected trio of locations.

Wu (Wu et al., 2021) The VRPs employ Transformers, a versatile tool widely used in deep learning applications (Tan et al., 2024; Hu et al., 2023a;b; 2022). Wu et al. (Wu et al., 2021) pioneered the integration of Transformers into VRPs. Positional embeddings within the encoder capture the linear structure of VRP solutions. Subsequently, the decoder computes location similarities, selecting the highest scores for 2-opt, swap, or insert operations.

Dact (Ma et al., 2021) Introducing an innovative dual-aspect collaborative Transformer for encoding locations, it incorporates a unique cyclic positional encoding. This feature effectively captures the circularity and symmetry inherent in Vehicle Routing Problems (VRPs).

NeuOpt (Ma et al., 2023) demonstrates prowess in executing flexible k-opt exchanges using a specialized action factorization method, comprising three key moves: S-move, I-move, and E-move. It utilizes a distinct recurrent dual-stream decoder tailored for decoding these exchanges. Moreover, NeuOpt incorporates a novel Guided Infeasible Region Exploration strategy to help the model navigate out of infeasible regions in Capacitated Vehicle Routing Problems (CVRPs).

NGM (Wang et al., 2021) is the inaugural learning-based approach to tackle Lawler’s QAPs. Initially crafted for resolving graph matching (GM) problems, NGM’s applications extend to diverse fields like video segmentation (Jiang et al., 2023). In addressing QAPs, NGM transforms them into a constrained vertex classification challenge on the association graph, denoted as \mathbf{K} . This graph emerges from the amalgamation of the flow and distance matrices, \mathbf{F} and \mathbf{D} , respectively, as per Equation 24.

$$\mathbf{K} = \mathbf{F} \otimes \mathbf{D} = \begin{bmatrix} f_{11}\mathbf{D} & \cdots & f_{1n}\mathbf{D} \\ \vdots & \ddots & \vdots \\ f_{m1}\mathbf{D} & \cdots & f_{mn}\mathbf{D} \end{bmatrix}. \tag{24}$$

The association graph is acquired through vertex classification by an embedding network, then normalized with Sinkhorn method, and trained end-to-end using cross-entropy loss.

RGM (Liu et al., 2022) is the inaugural RL technique to conquer the QAPLIB benchmark, capable of training sans ground truth. A revocable action framework enhances the agent’s adaptability for intricate constrained vertex classification tasks on association graphs.

E. Details of the MatNet*

We have repurposed MatNet, originally an L2C method for asymmetric TSPs and flexible flow shop problems, for our QAP tasks as an L2I method. Our adaptation, MatNet*, employs a dual-attention mechanism for encoding facility and location nodes (Figure 3). Following the approach in (Kwon et al., 2021), facility nodes start with 128-dimensional random initial embeddings, while location nodes begin with zero vectors of the same dimension. These, along with flow and distance matrices, undergo processing through three modules of a mixed-score transformer before input into our SAWT model for swap operations. However, this approach is computationally intensive due to the use of two transformers for encoding.

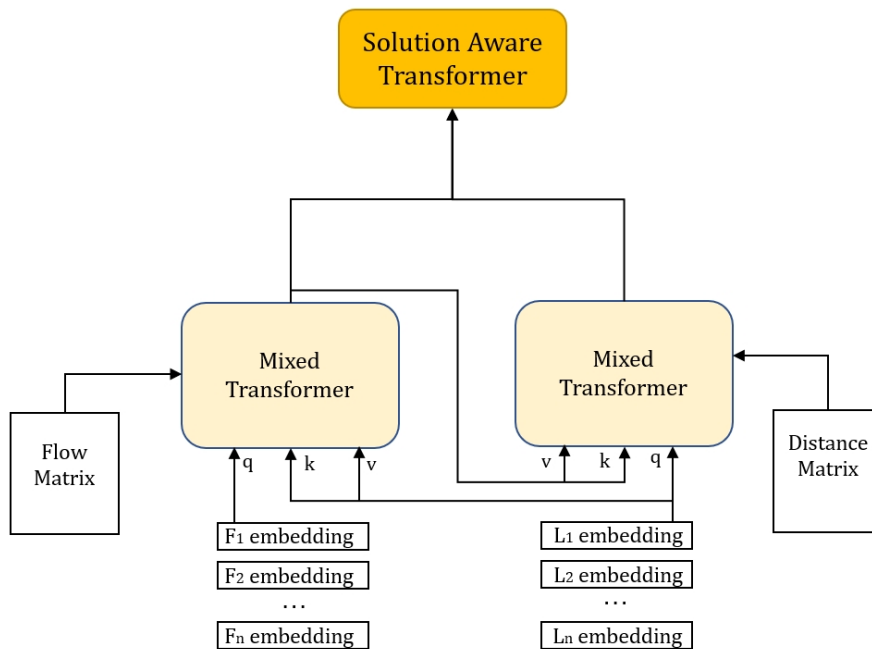
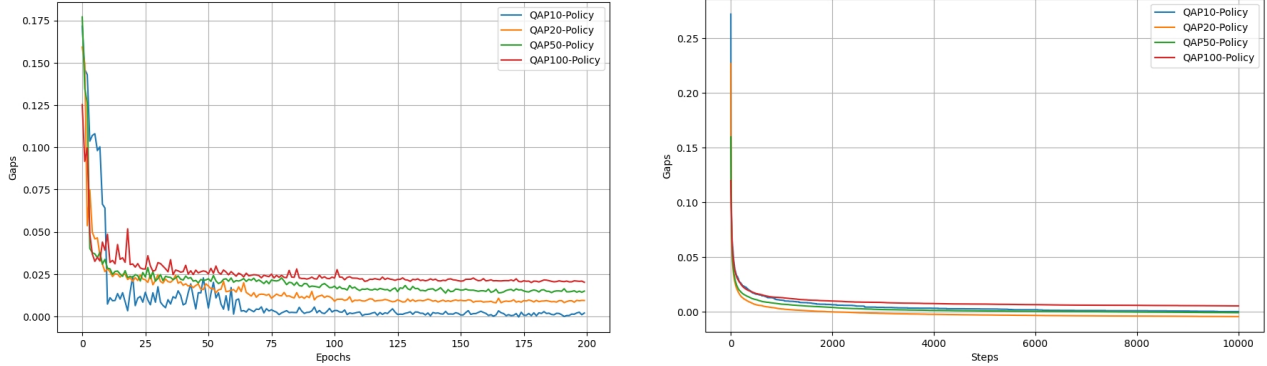


Figure 3. Structure of MatNet*.

F. More experimental results

F.1. Experiments with additional metrics

Two additional metrics are provided, standard deviation (Std) and winning rate, to assess SAWT. Following the methodology of (Costa et al., 2020), Std is computed across 512 testing instances for each QAP task. The winning rate is determined by comparing solution instances between SAWT and TS5K. Results are summarized in Tables 8 and 9. Key findings from Table 8 include: (1) SAWT exhibits superior performance, evidenced by lower median and reduced standard deviation. (2) RGM, utilizing the L2C method, shows higher standard deviation compared to L2I methods, indicating the robustness of L2I approaches. (3) Heuristic methods struggle with both median and standard deviation, highlighting challenges in achieving robust, optimal QAP solutions. Analysis from Table 9 reveals that while SAWT achieves better average objective values compared to TS5K, its winning rate against TS5K remains moderate. This suggests the existence of challenging instances for SAWT relative to TS5K.



(a) Gaps on 256 validation instances for 400 steps over training epochs. (b) Gaps on 256 testing instances over 10000 search steps.

Figure 4. Model behavior on training and testing period.

Table 8. Standard deviation experiments on QAP tasks.

METHODS	QAP 20	QAP50	QAP100
	MEAN ± STD	MEAN ± STD	MEAN ± STD
SM	70.07 ± 7.93	446.62 ± 22.85	1800.75 ± 61.21
RRWM	73.74 ± 8.56	457.40 ± 23.14	1823.76 ± 72.32
IPFP	75.52 ± 8.54	479.44 ± 23.66	1911.90 ± 72.54
COSTA	57.91 ± 6.98	404.28 ± 22.32	1720.62 ± 55.52
DACT	60.47 ± 7.04	418.77 ± 21.92	1743.82 ± 56.11
RGM	55.96 ± 7.51	–	–
SAWT	54.63 ± 6.68	379.96 ± 20.10	1617.23 ± 52.23

Table 9. Winning rate experiments on QAP tasks.

WINNING RATE	QAP10	QAP 20	QAP50	QAP100
SAWT	100.00%	72.26%	67.42%	10.15%

F.2. Additional experiments on QAP tasks

In Figure 4, we illustrate the optimal gap evolution for policies trained on QAP10, QAP20, QAP50, and QAP100, across training and testing phases. The gap, averaged over 256 validation instances across 400 search steps during training, and similarly over 256 testing instances across 10,000 search steps during testing, showcases a progressive narrowing throughout training epochs. Notably, Figure 4 (a) indicates larger instance sizes correlating with wider gaps, indicating increased difficulty levels. Additionally, Figure 4 (b) illustrates the swift gap minimization in the initial learning phases, transitioning to a more nuanced fine-tuning process as learning advances.

F.3. Additional experiments on TSP tasks

To test SAWT on solving MILPs, we conducted experiments on TSP tasks. Following (Ma et al., 2023), Our SAWT model was trained on self-generated datasets TSP20, TSP50, and TSP100. During inference, we searched for solutions over 10,000 steps and averaged the objective values. From Table 10, Our method proves comparable to Dact and surpasses AM and Costa, as indicated by the results. Although SAT performed less favorably than NeuOpt, it suggests the promising potential for SAT in TSP solving, considering SAT lacks modules tailored for TSPs. Considering that the compared baselines face extreme difficulties in solving QAP tasks as shown in Table 1, we highlight the importance of our work.

Table 11. Inference time of SAWT’s encoder, decoder and full model.

METHOD	QAP20			QAP50			QAP100		
	ENCODER	DECODER	FULL MODEL	ENCODER	DECODER	FULL MODEL	ENCODER	DECODER	FULL MODEL
SAWT{10k}	75.48s	26.84s	152s	77.85s	27.41s	160s	229.14s	85.52s	452s

Table 10. Experiments on TSP using SAWT. We train SAWT on TSP training data, and test it on the test data using 10000 search steps.

METHODS	TSP20		TSP50		TSP100	
	MEAN↓	GAP↓	MEAN↓	GAP↓	MEAN↓	GAP↓
AM	3.828	0.01%	5.699	0.05%	7.811	0.60%
COSTA	3.827	0.00%	5.703	0.12%	7.824	0.77%
DACT	3.827	0.00%	5.696	0.00%	7.772	0.10%
NEUOPT	3.827	0.00%	5.696	0.00%	7.766	0.02%
SAWT	3.827	0.00%	5.698	0.04%	7.782	0.22%

F.4. Inference time of SAWT

Table 11 demonstrates the runtimes for the SAWT encoder, decoder, and full model. Two key observations emerge: (1) The SAWT encoder’s runtime is nearly triple that of the decoder during inference, owing to its more intricate design. (2) The total runtime deviates from the sum of the encoder and decoder runtimes due to our model’s action sampling via the CPU and possible delays between the CPU and GPU.

F.5. Full experiments on QAPLIB

In this section, we present our generalization experiments to QAPLIB by directly applying our trained policy on QAP50. The results are shown in Table 13, and results are copied from NGM’s project ². There are four observations: (1) Our method is capable of solving all instances on a single GPU equipped with 12GB of memory. In contrast, as documented in (Wang et al., 2021), NGM requires more than 48GB of memory to solve a single instance when the size exceeds 150. This underscores the efficiency of our distinct encoding strategy. (2) Our methods surpass all the heuristics and learning-based methods in most of the instances. This proves the strong generalization ability of our SAWT model. (3) For large instances with *, our SAWT outperforms almost all the instances which further demonstrates the ability to solve large instances of our model. (4) For instances within the “Chr,” “Ste,” and “Esc” categories, the observed gaps are considerably substantial—for instance, 201.2% for “Chr20a” and 206.2% for “Esc128”—highlighting the limitations of our model.

F.6. Robustness analysis on QAPLIB

From Table 13, SAWT demonstrates a promising ability to tackle large-scale QAPs. For instance, our model can solve the “Tho150” using only 1 GB of GPU memory, a task at which RGM fails and NGM requires over 36GB of GPU memory. Instances marked with an asterisk (*) indicate RGM’s failure, typically on instances larger than 70. SAT excels in 86% (18 out of 21) of these large instances compared to NGM, a testament to its robustness on real-world large-scale datasets.

To delve deeper to understand the results in Table 2 and Table 13, we’ve integrated the flow matrix’s density statistics in Table 12, as it is one of the primary differences among datasets. In Section 6.1, we generate our flow matrix with a density value of $p = 0.7$, resulting in a relatively dense matrix. There are four observations: (1) Our model, SAWT, exhibits varying performance across different datasets with diverse flow matrix densities. Specifically, it struggles with “Chr”, “Kra”, “Ste”, and “Tho”, which have low flow matrix densities, indicating sensitivity to matrix density. Despite this, SAWT outperforms NGM and competes favorably with RGM, highlighting its robust QAP pattern learning ability. (2) Interestingly, SAWT performs well on “Esc” (29.6%) and “Scr” (38.8%), even with their low matrix densities. A closer look reveals that “Esc” has local density, which SAT perceives as a dense matrix, thereby improving performance. For instance, the flow matrix of “Esc16A” features a 10×10 dense matrix in the upper left corner, with only diagonal elements equal to zero. The remainder of the matrix’s elements are zero. “Scr” instances are simpler QAPs, as indicated by Gurobi’s quick optimal solutions (solved “Scr12”, “Scr15” within 1s and “Scr20” within 5min), which may explain SAWT’s fairly good performance. (3) SAWT generalizes well to datasets with high flow matrix densities, irrespective of different non-zero

²<https://thinklab.sjtu.edu.cn/project/NGM/index.html>

Table 12. Data distribution of QAPLIB.

	BUR	CHR	ESC	HAD	KRA	LIPA	NUG	ROU	SCR	SKO	STE	TAI(A/B)	THO	WIL
FLOW DENSITY	77.6%	15.2%	29.6%	91.6%	36.6%	89.2%	62.5%	90.2 %	38.8%	68.3%	26.5 %	88.8%/49.1%	48.2 %	87.9%

element distributions, illustrating its capacity to learn common QAP patterns. (4) A notable observation from Table 13 is SAWT’s better performance on “TaiA” (88.8%) compared to “TaiB” (49.1%), further underscoring its sensitivity to flow matrix density.

INSTANCE	UPPER BOUND	SM	RRWM	SINKHORN-JA	NGM	SAWT	GAP
BUR26A	5426670	6533340	6663181	5688893	5684628	5587628	2.9%
BUR26B	3817852	4690772	4741283	4053243	4063246	3903418	2.3%
BUR26C	5426795	6537412	6474996	5639665	5638641	5592521	3.1%
BUR26D	3821225	4649645	4678974	3985052	3994147	3951321	3.4%
BUR26E	5386879	6711029	6619788	5539241	5666202	5570198	3.4%
BUR26F	3782044	4723824	4814298	3979071	3954977	3868905	2.2%
BUR26G	10117172	12168111	12336830	10624776	10855165	10437749	3.1%
BUR26H	7098658	8753694	8772077	7453329	7670546	7344127	3.4%
CHR12A	9552	50732	43624	9552	27556	21046	120.4%
CHR12B	9742	46386	73860	9742	29396	19522	100.3%
CHR12C	11156	57404	50130	11156	34344	22966	105.1%
CHR15A	9896	77094	90870	11616	50272	19342	95.4%
CHR15B	7990	77430	115556	7990	52082	20014	152.2%
CHR15C	9504	64198	70738	9504	38568	20592	116.6%
CHR18A	11098	94806	115328	11948	83026	25808	132.5%
CHR18B	1534	4054	3852	2690	4810	3522	130.3%
CHR20A	2192	11154	13970	4624	10728	6615	201.2%
CHR20B	2298	9664	14168	3400	9962	5998	161.0%
CHR20C	14142	112406	195572	40464	115128	41146	190.9%
CHR22A	6156	16732	15892	9258	16410	7085	15.1%
CHR22B	6194	13294	13658	6634	15876	7488	20.8%
CHR25A	3796	21526	32060	5152	18950	4126	8.6%
ELS19*	17212548	33807116	74662642	18041490	34880280	21825512	26.8%
ESC16A	68	98	80	100	88	68	0.0%
ESC16B	292	318	294	304	308	296	1.3%
ESC16C	160	276	204	266	184	162	1.2%
ESC16D	16	48	44	58	40	16	0.0%
ESC16E	28	52	50	44	48	32	14.2%
ESC16F	0	0	0	0	0	0	0.0%
ESC16G	26	44	52	52	50	26	0.0%
ESC16H	996	1292	1002	1282	1036	1030	3.4%
ESC16I	14	54	28	36	26	18	28.5%
ESC16J	8	22	18	18	16	8	0.0%
ESC32A	130	426	240	456	428	212	63.0
ESC32B	168	460	400	416	424	252	50.0%
ESC32C	642	770	650	886	844	650	1.2%
ESC32D	200	360	224	356	288	246	23.0%
ESC32E	2	68	6	46	42	2	0.0%
ESC32G	6	36	10	46	28	10	63.3%
ESC32H	438	602	506	–	592	530	21.0%
ESC64A	116	254	124	276	250	190	63.7%
ESC128*	64	202	78	–	238	196	206.2%
HAD12	1652	1894	2090	–	1790	1696	2.6%
HAD14	2724	3310	3494	2916	2922	2826	3.7%
HAD16	3720	4390	4646	3978	4150	3854	3.6%
HAD18	5358	6172	6540	5736	5780	5574	4.0%
HAD20	6922	8154	8550	7464	7334	7372	6.5%
KRA30A	88900	148690	136830	125290	114410	117436	32.1%
KRA30B	91420	150760	141550	126980	118130	117110	28.1%
KRA32	88700	145310	148730	128120	121340	119036	34.2%

Learning Solution-Aware Transformers for Efficiently Solving Quadratic Assignment Problem

INSTANCE	UPPER BOUND	SM	RRWM	SINKHORN-JA	NGM	SAWT	GAP
LIPA20A	3683	3956	3940	3683	3929	3683	0.0%
LIPA20B	27076	36502	38236	27076	33907	27076	0.0%
LIPA30A	13178	13861	13786	13178	13841	13178	0.0%
LIPA30B	151426	198434	201775	151426	192356	151426	0.0%
LIPA40A	31538	32736	32686	31538	32666	31538	0.0%
LIPA40B	476581	628272	647295	476581	616656	476581	0.0%
LIPA50A	62093	64070	64162	62642	64100	62093	0.0%
LIPA50B	1210244	1589128	1591109	1210244	1543264	1241710	2.6%
LIPA60A	107218	109861	110468	108456	110094	107218	0.0%
LIPA60B	2520135	3303961	3300291	2520135	3269504	2578098	2.3%
LIPA70A*	169755	173649	173569	172504	173862	173153	2.0%
LIPA70B*	4603200	6055613	6063182	4603200	5978316	4603200	0.0%
LIPA80A*	253195	258345	258608	257395	258402	257778	1.8%
LIPA80B*	7763962	10231797	10223697	7763962	10173155	7763962	0.0%
LIPA90A*	360630	367384	367370	366649	367193	366573	1.6%
LIPA90B*	12490441	16291267	16514577	12490441	16194745	12490441	0.0%
NUG12	578	886	1038	682	720	602	4.1%
NUG14	1014	1450	1720	-	1210	1068	5.3%
NUG15	1150	1668	2004	1448	1482	1234	7.3%
NUG16A	1610	2224	2626	1940	1836	1738	7.9%
NUG16B	1240	1862	2192	1492	1580	1340	8.0%
NUG17	1732	2452	2934	2010	2004	1906	10.0%
NUG18	1930	2688	3188	2192	2312	2128	10.2%
NUG20	2570	3450	4174	3254	2936	2826	9.9%
NUG21	2438	3702	4228	3064	2916	2680	10.0%
NUG22	3596	5896	6382	3988	4616	3956	10.1%
NUG24	3488	4928	5720	4424	4234	3844	10.5%
NUG25	3744	5332	5712	4302	4420	4126	10.4%
NUG27	5234	7802	8626	6244	6332	5810	11.1%
NUG28	5166	7418	8324	6298	6128	5734	11.0%
NUG30	6124	8956	10034	7242	7608	6926	13.1%
ROU12	235528	325404	377168	276446	321082	254842	8.2%
ROU15	354210	489350	546526	390810	469592	393882	11.2%
ROU20	725522	950018	1010554	823298	897348	820566	13.1%
SCR12	31410	71392	95134	45334	44400	34614	10.2%
SCR15	51140	104308	101714	74632	81344	65102	27.3%
SCR20	110030	263058	350528	171260	182882	162846	48.0%
SKO42	15812	20770	23612	19058	20192	18660	18.7%
SKO49	23386	29616	34548	27160	28712	27292	16.7%
SKO56	34458	44594	49650	40954	42182	40662	18.0%
SKO64	48498	60878	65540	55738	60368	57034	17.6%
SKO72*	66256	82156	89264	76332	79716	76508	15.4%
SKO81*	90998	112838	118372	105246	107588	104726	15.0%
SKO90*	115534	140840	148784	133818	137402	132270	14.4%
SKO100A*	152002	185738	184854	176626	180972	173798	14.3%
SKO100B*	153890	185366	189502	177398	180774	176576	14.7%
SKO100C*	147862	178710	188756	169566	175740	169290	14.4%
SKO100D*	149576	181328	186086	170648	175096	170964	14.3%
SKO100E*	149150	180062	192342	171656	176010	170858	14.5%
SKO100F*	149036	177518	189284	171296	173552	170404	14.3%

INSTANCE	UPPER BOUND	SM	RRWM	SINKHORN-JA	NGM	SAWT	GAP
STE36A	9526	30030	33294	17938	16648	13972	46.7%
STE36B	15852	176526	193046	47616	43248	42956	170.9%
STE36C	8239110	24530792	28908062	14212212	12988352	13418384	62.9%
TAI12A	224416	318032	392004	245012	259014	249102	11.1%
TAI12B	39464925	96190153	124497790	81727424	65138752	46173962	16.9%
TAI15A	388214	514304	571952	471272	467812	390155	0.5%
TAI15B	51765268	702925159	702292926	52585356	495479040	52718274	1.7%
TAI17A	491812	669712	738566	598716	630644	559682	13.8%
TAI20A	703482	976236	1012228	849082	896518	794934	12.9%
TAI20B	122455319	394836310	602903767	220470588	237607744	139599064	14.0%
TAI25A	1167256	1485502	1536172	1341104	1393248	1371526	17.5%
TAI25B	344355646	764920942	1253946482	798113083	730775168	512056846	48.7%
TAI30A	1818146	2210304	2305048	2072218	2065706	1930871	6.2%
TAI30B	637117113	1008164383	1766978330	1114514832	1359600384	828252247	30.0%
TAI35A	2422002	3030184	3100748	2820060	2886132	2669068	10.2%
TAI35B	283315445	454981851	574511546	446783959	455718176	360377246	27.2%
TAI40A	3139370	3825396	3985684	3547918	3610604	3619378	15.2%
TAI40B	637250948	1165811212	1423772477	1019672934	1053339520	900201547	41.2%
TAI50A	4938796	6078426	6203546	5569952	5891066	5590717	13.2%
TAI50B	458821517	796553600	790688128	696556852	764856128	632256050	37.8%
TAI60A	7205962	8614998	8731620	8243624	8596094	8230248	14.2%
TAI60B	608215054	1089964672	1279537664	978843717	994559424	801450909	31.7%
TAI64C	1855928	5893540	6363888	3189566	5703540	2080496	12.1%
TAI80A*	13499184	15665790	16069786	15352662	15648708	15279496	13.1%
TAI80B*	818415043	1338090880	1410723456	1215586531	1275809408	1108782694	35.4%
TAI100A*	21052466	24176962	24446982	23787764	24077728	23576714	11.9%
TAI100B*	1185996137	1990209280	2192130048	1589275900	1853681152	1677867703	41.4%
TAI150B*	498896643	662657408	755505920	-	653429440	627949553	25.8%
THO30	149936	230828	267194	202844	187062	184722	23.2%
THO40	240516	375154	440146	314070	313026	304012	26.4%
THO150*	8133398	10000616	10689758	9508422	9702946	9595620	17.9%
WIL50	48816	56588	60420	54030	55390	52700	8.1%
WIL100*	273038	305030	307258	292118	295418	294568	7.8%

Table 13. The * in the Table means the instances RGM fails to solve due to the large size of the instances. We do not add the RGM method for the reason that the author does not reveal the independent results on each instance. The instances tested both on RGM and SAWT results in a mean average of 35.8% and 26.8% which demonstrates the effectiveness of our SAWT. Some instances like “Chr” and “Ste” perform poorly on the SAWT, showing the limitation of our model’s generalization ability.